X-ray flare in XRF 050406: evidence for prolonged engine activity

P. Romano*, A. Moretti*, P.L. Banat*, D.N. Burrows†, S. Campana*, G. Chincarini*, S. Covino*, D. Malesani**, G. Tagliaferri*, A.D. Falcone†, M. Capalbi‡, G. Cusumano§, P. Giommi‡, V. La Parola§, V. Mangano§, M. Perri‡ and C. Pagani*

*INAF–Osservatorio Astronomico di Brera, Via E. Bianchi 46, I-23807 Merate (LC), Italy
†Department of Astronomy & Astrophysics, Pennsylvania State University, PA 16802, USA
**International School for Advanced Studies (SISSA-ISAS), Via Beirut 2-4, I-34014 Trieste, Italy
‡ASI Science Data Center, via G. Galilei, I-00044 Frascati (Roma), Italy
§INAF–IASF, Via U. La Malfa 153, I-90146 Palermo, Italy

Abstract.
We present observations of XRF 050406, an X-ray flash with a relatively low fluence ($\sim 10^{-7}$ erg cm^{-2} in the 15–350 keV band), a soft spectrum (photon index $\Gamma_\gamma = 2.65$), no significant flux above ~ 50 keV and a peak energy $E_\mathrm{p} < 15$ keV. XRF 050406 is the first burst detected by Swift clearly showing a flare in its X-ray light curve. The flare peaks 210 s after the BAT trigger, presents a flux variation $\delta F/F \sim 6$ in a timescale $\delta t/t_\mathrm{peak} \ll 1$ and a measured fluence of 1–15% of the prompt one. We argue that the producing mechanism is late internal shocks, which implies that the central engine is still active at 210 s, though with a reduced power with respect to the prompt emission. The X-ray light curve flattens to a more shallow slope with a decay index of ~ 0.5 after ~ 4400 s, also supporting continued central engine activity.

Keywords: Gamma rays: bursts; X-rays: bursts; X-rays: individuals (XRF 050406)
PACS: 98.70.Rz,98.70.Qy

DATA ANALYSIS

We present the XRT observations of the first Swift burst where a flare is clearly detected in its X-ray light curve [1, 2], during which the source count rate increased by a factor of ≥ 6. This feature had never been observed before in Swift data, and had rarely been observed before in any X-ray afterglow [3].

On 2005 Apr 6 at 15:58:48.40 UT, the Swift-BAT [4] triggered on GRB 050406 [5]. The Swift-XRT [6] observations of XRF 050406 started on 2005 Apr 6 at 16:00:12 UT, only 84 s after the trigger, and ended on 2005 Apr 22, thus summing up a total net exposure (in PC mode) of ~ 163 ks spread over a $\sim$16 d baseline. Full details (especially about the data) can be found in Romano et al. [2].

Figure 1 shows the background-subtracted 0.2–10 keV light curve with the BAT trigger as origin of time. It clearly shows a complex behavior, with a power law decay underlying a strong flare which peaks at ≈ 210 s after the BAT trigger. Using the BAT trigger as reference time and excluding the data taken during the flare ($180\,\mathrm{s} < t < 300\,\mathrm{s}$), a fit with a broken power law yields slopes $\alpha_1 = 1.58^{+0.18}_{-0.16}$ and $\alpha_2 = 0.50 \pm 0.14$, and a break at ~ 4200 s. As a reference, the 0.2–10 keV unabsorbed flux at t_b is $(4 \pm 1) \times 10^{-13}$

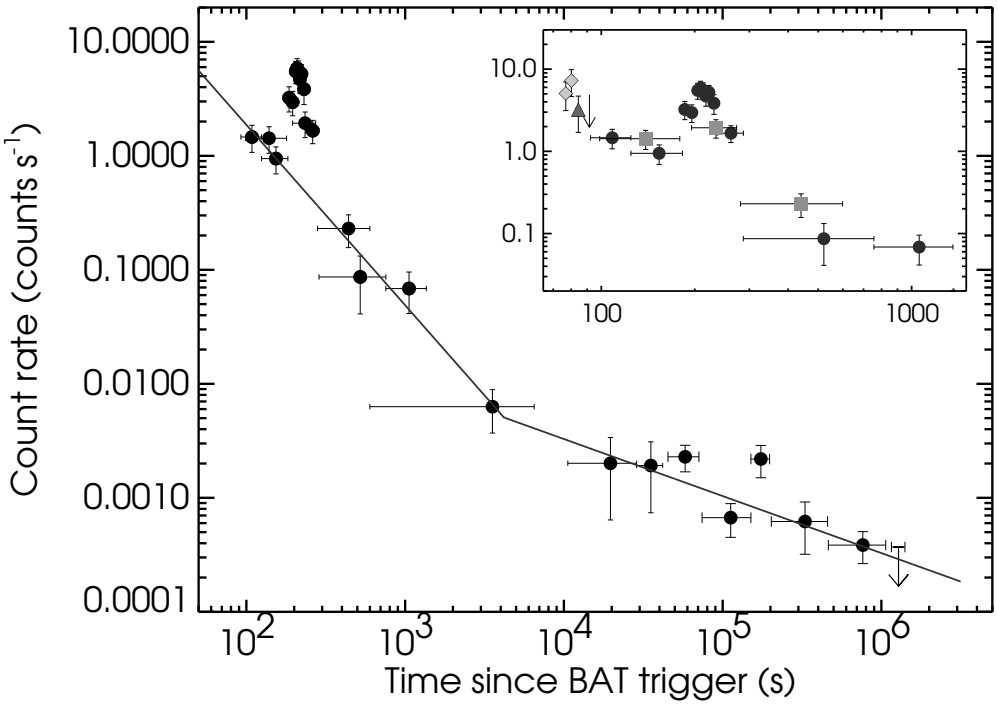

FIGURE 1. Background-subtracted X-ray light curve of the XRF 050406 afterglow in the 0.2–10 keV energy band, with time referred to the BAT trigger, 2005 Apr 06 at 15:58:48.4 UT. For $t < 4 \times 10^4$ s we binned the source counts with a minimum of 30 counts per time bin, and dynamically subtracted the normalized background counts in each bin. Afterwards, we used `XIMAGE` with the option `SOSTA`, which calculates vignetting- and PSF-corrected count rates within a specified box, and the background in a user-specified region. The last point after 10^6 s is a 3-σ upper limit. The inset shows the details of the first $\sim$ 1000 s, including data in all XRT modes. The diamonds represent LrPD mode data taken during the latter portion of the slewing phase; the triangle is the initial IM point (84 s after the trigger), the downward-pointing arrow is a LrPD limit (pointing, 91 s after the trigger), the circles are WT mode data (starting from 92 s after the trigger), and the squares are PC mode data (starting from 99 s after the trigger). The data have been corrected for pile-up (where appropriate) and PSF losses. The solid line represents the best-fit broken power-law model to the light curve (excluding the flare).

erg cm^{-2} s^{-1} and the luminosity in the 0.7–34.4 keV band is $(1.9 \pm 0.9) \times 10^{46}$ erg s^{-1} for $z = 2.44 \pm 0.36$ [7]. Both the rising and the falling part of the flare had very steep slopes that, when fit with a simple power law, yield $\alpha_{1,\mathrm{flare}} = -6.8^{+2.4}_{-2.1}$ and $\alpha_{2,\mathrm{flare}} = 6.8^{+3.6}_{-2.0}$ and the peak is at 213 ± 7 s from the BAT trigger (after the underlying power-law afterglow is subtracted). The flare can also be parameterised as a Gaussian with a peak at $211.1^{+5.4}_{-4.4}$ s and a width of $17.9^{+12.3}_{-4.6}$ s. The ratio of the characteristic time-scale and the peak time is $\delta t / t_{\mathrm{peak}} \ll 1$, which puts severe constraints on the emission mechanisms that can produce the flare. Integration of the Gaussian best-fitting function yields an estimate of the fluence of the flare, $(1.4 \pm 1.0) \times 10^{-8}$ erg cm^{-2}, corresponding to an energy of $(2.0 \pm 1.4) \times 10^{50}$ erg.

The photon index is $\Gamma_{\mathrm{X}} = 2.1 \pm 0.3$ and does not vary throughout the observation. Since the afterglow of XRF 050406 was very faint, it was not possible to perform time-

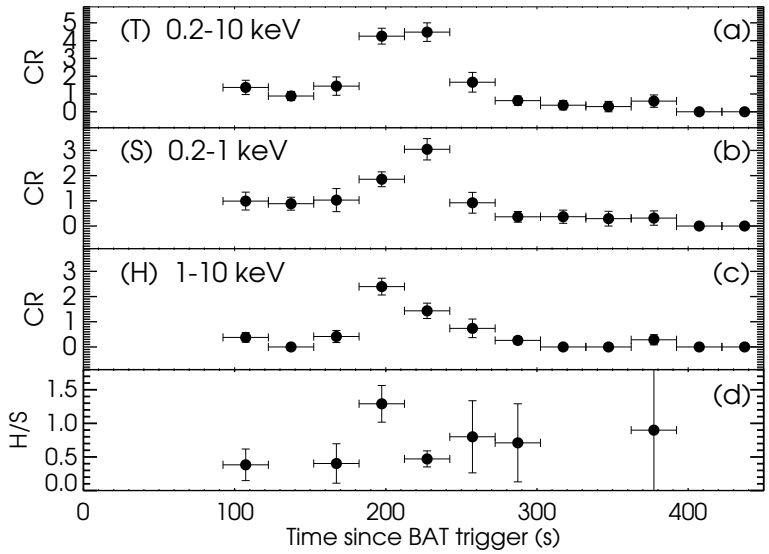

FIGURE 2. Windowed-timing background-subtracted light curves: total band (**T**, 0.2–10 keV, panel **(a)**), soft band (**S**, 0.2–1 keV, **(b)**), and hard band (**H**, 1–10 keV, **(c)**). The last panel **(d)** is the ratio of hard to soft count rates.

resolved spectroscopy to distinguish the spectral properties of the afterglow proper from the ones of the flare. Therefore, to test for spectral evolution we extracted events from the WT data in two more energy bands, 0.2–1 keV (soft, S) and 1–10 keV (hard, H), as well as the total band, 0.2–10 keV (Figure 2). During the rising portion of the flare the hard band flux increases by a factor of ≥ 6 while the soft band flux only increases slightly, so that the spectrum of the flare starts off harder than the underlying afterglow, and then evolves into a softer state as its flux decreases; this can be seen in the following time bin, when the soft band flux peaks with a flare to pre-flare flux ratio of ~ 3.5. Indication of spectral evolution during the flare comes as a ~ 3-σ excess over a constant fit to the hardness ratio H/S. It should be noted that this behavior is reminiscent of that observed in the prompt emission, with the harder band peak preceding the softer band peak. At $t \sim 1.7 \times 10^5$ s a second faint bump is detected as a 2-σ excess over the underlying afterglow.

DISCUSSION

XRF 050406 is classified as an X-ray flash, with a 15–350 keV fluence $\sim 1 \times 10^{-7}$ erg cm^{-2}, a soft spectrum ($\Gamma_\gamma = 2.65$), no significant flux above ~ 50 keV and a peak energy $E_{\rm p} < 15$ keV. The isotropic-equivalent gamma-ray energy of this event is $E_{\rm iso} = (1.4^{+1.6}_{-0.6}) \times 10^{51}$ erg, and this effectively puts XRF 050406 in the low-energy tail of GRB energies [8]. Its main characteristics are however not qualitatively different from those of normal GRBs. The observed X-ray photon index ($\Gamma_{\rm X} = 2.1$) is common among X-ray afterglows [9]. The light curve shows a break from a relatively steep decay ($\alpha_1 = 1.58$) to a flatter one ($\alpha_2 = 0.50$). Its overall shape is similar to the one typically

observed by the XRT [9, 10], even though the initial slope is less steep than average. As observations accumulate, it becomes clear that these two classes of phenomena share many properties, and both have afterglows with similar characteristics. This is a clue that both events may have a common origin.

XRF 050406 is the first Swift-detected burst that showed a prominent flare in its X-ray light curve. A promising mechanism to produce the flare is late internal shocks [11], which implies that the central engine is still active at $t = 210$ s, even though the prompt emission ended after $t \sim 6$ s. The late-time activity in this case must have a reduced power with respect to the prompt emission, as the relative fluences indicate. Such a mechanism would naturally explain the steep rise and decay slopes. The indications of spectral evolution throughout the flare further support this interpretation. The flare appears to be harder than the underlying afterglow, which suggests a distinct origin for this emission. Furthermore, there are indications of spectral evolution, which shows the typical hard-to-soft pattern. Such a behavior is commonly observed in the prompt emission spikes of GRBs, which are produced in internal shocks. Further evidence of late engine activity comes from both the flat part of the light curve and possibly by the presence of the late-time bump observed at $t \sim 1.7 \times 10^5$ s.

We now know that flaring is quite a common behaviour, since ~ 50 % of the bursts detected by XRT which were promptly observed showed flares. All the characteristics of the XRF 050406 flares have now been observed in most flaring GRBs, as well [12]. For example, highly significant spectral evolution throughout the flare has been reported in GRB 050502B, which was the brightest observed so far [13] and GRB 050724 [14]. In several cases the flares present large amplitudes and occur on short timescales. Furthermore, several flares are often observed in the same event, at times ranging from ~ 100 to 10^4–10^5 s after the burst. Finally, in most cases the afterglow is clearly present *before* the onset of the flare, and has consistent decay slope and flux levels with after the flare. The present case shows that flares are present both in XRFs and in GRBs indicating that flares are linked to some common properties of both kinds of bursts, and probably tied to their central engine.

REFERENCES

1. D. N. Burrows, P. Romano, A. Falcone, and et al., *Science* **309**, 1833–1835 (2005).
2. P. Romano, A. Moretti, P. L. Banat, and et al., *Astronomy and Astrophysics* **in press** (2006).
3. L. Piro, M. De Pasquale, P. Soffitta, and et al., *The Astrophysical Journal* **623**, 314–324 (2005).
4. S. D. Barthelmy, and et al., *Space Science Review* **120**, 143 (2005).
5. A. Parsons, S. Barthelmy, J. Cummings, and et al., *GRB Coordinates Network* **3180**, 1 (2005).
6. D. N. Burrows, J. E. Hill, Nousek, and et al., *Space Science Review* **120**, 165 (2005).
7. P. Schady, K. A. Mason, J. P. Osborne, and et al., *The Astrophysical Journal* **in press** (2006).
8. J. S. Bloom, D. A. Frail, and S. R. Kulkarni, *The Astrophysical Journal* **594**, 674–683 (2003).
9. G. Chincarini, A. Moretti, P. Romano, and et al. (2005), `arXiv:astro-ph/0506453`.
10. J. A. Nousek, C. Kouveliotou, D. Grupe, and et al., *The Astrophysical Journal* **in press** (2006).
11. B. Zhang, Y. K. Fan, J. Dyks, and et al., *The Astrophysical Journal* **in press** (2006).
12. D. N. Burrows, P. Romano, O. Godet, and et al. (2005), `arXiv:astro-ph/0511039`.
13. A. D. Falcone, D. N. Burrows, D. Lazzati, and et al., *The Astrophysical Journal* **in press** (2006).
14. S. Campana, G. Tagliaferri, D. Lazzati, and et al., *Astronomy and Astrophysiscs* **submitted** (2006).